THREE-PHASE SATURATION MEASUREMENT DURING GRAVITY DRAINAGE AND TERTIARY WATERFLOOD: IMPROVEMENT OF DUAL ENERGY GAMMA-RAY ATTENUATION TECHNIQUE

C.CAUBIT[1], H.BERTIN[1], G.HAMON[2]
1.TREFLE-ENSAM, University of Bordeaux, France 2.TOTAL, France

This paper was prepared for presentation at the International Symposium of the Society of Core Analysts held in Abu Dhabi, UAE, 5-9 October, 2004

ABSTRACT

In petroleum engineering, three-phase flow configurations occur in many situations, tertiary water or gas flood, water alternating gas process (W.A.G)... Information on residual saturation (oil and gas) during three-phase flow is crucial for reservoir engineering studies.
In this study, a dual energy device designed to improve the accuracy of saturation measurement during three-phase flow is presented. The two sources (Am^{241} and Cs^{137}) are situated one above the other in front of two separate small size new generation detectors. Therefore, attenuation measurements of each source are measured independently optimizing the performance of the detectors for each energy and avoiding a Compton effect correction.
A gas-oil gravity drainage experiment followed by a tertiary waterflood performed on a long, intermediate-wet core is also presented. In situ saturation measurement using the gamma-ray attenuation technique was optimized for all stages of the experiment. This test was designed to provide two and three-phase data on the same core during the same experiment. Good agreement between local saturation measurement and global mass balance versus time was obtained confirming the reliability of the dual energy device.
Moreover, a technique for the estimation of the accuracy of local in-situ data is described. This technique was based on linear and covariance methods showing that (i) accuracy is saturation dependent, more accurate values being obtained when gas saturation is high, (ii) water and gas saturation profiles are more accurate than oil saturation profiles. Therefore, an improved measurement procedure depending on flow conditions (two or three-phase, dynamic or static conditions) was developed in order to optimize accuracy measurements.

INTRODUCTION

A good understanding of multiphase flow in porous media needs to determine certain properties: capillary pressure, P_c, and relative permeability k_r. Moreover P_c and k_r are saturation dependent hence the importance of having laboratory devices to measure *in situ* saturation. In addition, *in situ* saturation measurement permits direct observation of phenomenon such as saturation gradient and/or end effect.
In this study, porosity and two or three phase saturation profile measurement are examined. *In situ* saturation and porosity measurement devices can be divided roughly into two categories. First are the apparatus providing 3D imaging of porosity and saturation profiles such as CT Scan and Magnetic Resonance Imaging (M.R.I) techniques. The CT Scan

technique is very efficient for porosity, two and three-phase saturation measurement while M.R.I allows only porosity and two-phase measurement. Disadvantages of these techniques are the price of the apparatus and their maintenance. Moreover, it is not easy to perform lengthy experiments in a vertical position such as gravity drainage.
The second category of saturation measurement devices use techniques which provide average values over a given measurement volume. It includes the use of nuclear tracer [Naylor et al. 1989] gamma ray attenuation techniques [Nichols et al., 1989], [Barroux et al. 1991] and X-ray attenuation techniques [Oak et al. 1988]. These techniques are operational for three-phase flow configurations when two different energy levels are available and commonly used in petroleum engineering research laboratories for three-phase flow studies. Dual techniques using one gamma source combined with resistivity measurements has given [Vizika et al., 1995] accurate results.
In the present study, dual energy gamma-ray attenuation was chosen to perform three-phase saturation measurements for the following reasons: vertical and horizontal fluid displacement can be performed easily on a long core (1m); compared to techniques using nuclear tracers, there is no problem concerning the radioactive effluents; moreover this technique is less expensive than techniques using X-ray tubes (CT Scan and X-ray attenuation). A dual energy gamma-ray apparatus to measure in situ saturation during gravity drainage followed by a tertiary water flood is presented here.
First, gamma radiation theory is briefly presented and the computation of porosity, two- and three-phase saturation, and their accuracy is detailed. Secondly, an example of experimental data and accuracy measurement is presented.

THEORY

Gamma-ray attenuation

Gamma-radiations

Gamma-radiation is made up of electromagnetic waves whose wave lengths range from 10^{-10}m and 10^{-13}m. This radiation can be emitted by natural or artificial sources when the nuclei of a radionuclide jump from an excited state of energy towards another more stable state of energy. Photons are emitted during this stage called radioactive decay, following a statistical process that can be approximated by a Poisson's distribution.
A radioactive source can be characterised by its activity A, expressed in Becquerel (Bq), its energy E, expressed in electronvolt (eV) and half-life period , $T_{1/2}$. Activity is a function of time and can be expressed as follow:

$$A(t) = A_0 \exp(-\lambda t) \quad (1)$$

where A_0 is the initial activity and λ the probability that a nucleus will decay in the next second. Half-life period, $T_{1/2}$, which is the time lapse for which radionuclide activity, A(t), decreases by a factor of two is defined as follow:

$$\frac{A(t)}{A_0} = \frac{1}{2} = \exp(-\lambda T_{1/2}) \quad (2)$$

When radiation penetrates matter, photons may be removed from the incident beam by different interactions which produce a photoelectric effect, Compton scattering and pair production [Tait, 1980]. This phenomenon is called attenuation and can be modelled by Beer's law.

Attenuation of gamma radiation: Beer's law

Considering a homogeneous absorbing medium with a density ρ, a thickness dx and a incident photon intensity I (eV), it is possible to determine the differential dI:

$$dI = -\alpha I dx \quad (3)$$

where α is the mass attenuation coefficient (m^2g^{-1}), which depends on the chemical structure of the medium and the incident beam energy. Moreover, the intensity I and the counting N are linked by:

$$I = h\nu N \quad (4)$$

where h is the Planck constant and ν the radiation frequency. Equation (3) and (4) lead to:

$$N = N_0 \exp(-\alpha\rho x) \quad (5)$$

where N_0 and N correspond to the emitted radiation of the radioactive source and the transmitted radiation through an absorbing homogeneous medium, respectively. This exponential law can be extended for heterogeneous media:

$$N = N_0 \exp(-\sum_i \alpha_i \rho_i x_i) \quad (6)$$

where α_i, ρ_i and x_i define for each phase, the mass attenuation coefficient, density and length. In the present application, the linear attenuation coefficient ($\xi=\rho\alpha$) was used; thus Equation (6) becomes:

$$N = N_0 \exp(-\sum_i \xi_i x_i) \quad (7)$$

MEASUREMENT APPARATUS AND ACCURACY CONCERNS

Dual energy apparatus

The apparatus is composed of three main elements: the two radiation sources, the source-holder and counting devices and the displacement rig.

Radioactive sources: The radioactive sources used were Americium 241 and Caesium 137 (Am^{241} and Cs^{137}), their properties are given on the Table 1. These sources were chosen because of their pronounced energy level difference necessary for the measurement of three-phase saturation. Moreover, these sources have been commonly used in the literature [Barataud et al., 1972], [Barroux et al., 1991] and [Stroosnijder et al., 1974].

Source-holder: The apparatus represented in Figure 1 is composed of the two gamma-ray sources placed one above the other in a lead holder. The two source axes are separated by a distance of 13 mm. Two 95mm long, 5mm diameter lead collimators are located in front of the sources. In front of the source holder two counting devices, photomultiplier and crystal scintillator (NaI(Tl)), are located behind two 85mm long, 5mm diameter, lead collimators. The source holder and counting device collimators are on the same axes.

Displacement rig: The source holder and counting devices are moved by a 2D (1m×1m) displacement rig using step by step engines whose resolution is equal to 1μm.

Americium and Caesium: the Compton effect

Most dual energy systems described in the literature (Barataud et al., 1999, Barroux et al., 1991) consist of two sources, (Am^{241} and Cs^{137}), the higher energy level source being behind the lower energy level source. In this case, the Compton effect due to the higher energy level source influences the lower energy level source spectrum and a counting correction formula should be used [Nofziger et al, 1974], [Ferrand et al, 1986], [Angulo-Jamarillo, 1989]. Other dispositions with two perpendicular gamma beams [Stroosnijder et al, 1974] have been used, but they assume that the porous medium is homogeneous and

isotropic. In the present system the two sources and counting devices are separated and the Caesium Compton effect does not affect the Americium spectrum. The same porous medium location can be counted twice by merely moving the rig.

BASIC EQUATIONS: APPLICATION TO POROUS MEDIA

Porosity and saturation were defined as follows:

$$\Phi = \frac{V_P}{V_T} \text{ and } S_i = \frac{V_i}{V_P} \tag{8}$$

where V_P, V_T and V_i represent the pore volume, the total volume of the porous medium and the volume occupied by the phase i, respectively.

For the present study, local saturation and porosity of cylindrical volumes corresponding to the collimated gamma-ray beam were determined.

$$\Phi = \frac{S_b x}{S_b l} \Rightarrow \Phi = \frac{x}{l} \text{ and } S_i = \frac{S_b x_i}{S_b l \Phi} \Rightarrow S_i = \frac{x_i}{l\Phi} \tag{9}$$

where x, x_i, l and S_b are the equivalent length of the pore space, the equivalent length of the path of gamma-ray through the phase i in multiphase flow, the total length of the porous medium and the area of the gamma-ray beam, respectively. Then, by applying the Beer's law to the dry, fully brine saturated porous medium, two- and three-phase configuration one obtains:

For j=Am, Cs
$$N_1^j = N_0^j \exp(-\xi_s^j x_s - \xi_g^j x_g) \tag{10}$$

For j=Am, Cs
$$N_2^j = N_0^j \exp(-\xi_s^j x_s - \xi_w^j x_w) \tag{11}$$

For j=Am, Cs
$$N_3^j = N_0^j \exp(-\xi_s^j x_s - \xi_w^j x_w - \xi_o^j x_o) \tag{12}$$

For j=Am, Cs
$$N_4^j = N_0^j \exp(-\xi_s^j x_s - \xi_w^j x_w - \xi_o^j x_o - \xi_g^j x_g) \tag{13}$$

where indexes 1, 2, 3 and 4 correspond to the dry, brine saturated, two-phase, and three-phase configurations, respectively; s, g, w and o are the solid, the gas (air), the water (brine) and the oil phases, respectively. Porosity and saturation were computed assuming that ξ_g is negligible compared to ξ_o and ξ_w.

Moreover, the saturation equations for two-phase (oil/water) and three phase (oil/water/gas) configurations were:

$$S_o + S_w = 1 \tag{14}$$

$$S_o + S_w + S_g = 1 \tag{15}$$

where S_o, S_w and S_g are the oil, water and gas saturation, respectively.

Porosity measurement

Porosity ϕ was determined from equation (9) to (11):

For j=Am, Cs
$$\Phi^j = \frac{1}{\xi_w^j l} \ln\left(\frac{N_1}{N_2}\right)^j \tag{16}$$

Saturation measurement

Two phase flow (water/oil)

Oil saturation was determined from Equations (9), (10), (11) and (14):

For j=Am, Cs
$$S_o^{j2\varphi} = \frac{1}{\left(\xi_o^j - \xi_w^j\right) l\Phi^j} \ln\left(\frac{N_1}{N_3}\right)^j \tag{17}$$

Then water saturation was given by the saturation Equation (14).

Three phase flow

Oil saturation was computed from Equations (9), (10), (13) and (15):
$$S_o^{3\varphi} = A\left[B\ln\left(\frac{N_1}{N_4}\right)^{Am} - C\ln\left(\frac{N_1}{N_4}\right)^{Cs}\right] \tag{18}$$

where
$$A = \frac{1}{\xi_o^{Am}\xi_w^{Cs} - \xi_o^{Cs}\xi_w^{Am}} \;;\; B = \frac{\xi_w^{Cs}}{l\Phi^{Am}} \;;\; C = \frac{\xi_w^{Am}}{l\Phi^{Cs}} \tag{19}$$

$$S_w^{3\varphi} = A\left[B^*\ln\left(\frac{N_1}{N_4}\right)^{Am} - C^*\ln\left(\frac{N_1}{N_4}\right)^{Cs}\right] \tag{20}$$

where
$$A = \frac{1}{\xi_o^{Am}\xi_w^{Cs} - \xi_o^{Cs}\xi_w^{Am}} \;;\; B^* = \frac{\xi_o^{Cs}}{l\Phi^{Am}} \;;\; C^* = \frac{\xi_o^{Am}}{l\Phi^{Cs}} \tag{21}$$

Then gas saturation was determined using Equation (15).

Measurement accuracy

Measurement accuracy was determined using two methods:

Differential method (DM): If one considers a function of n variables $F(x_1, x_{2,\ldots,} x_n)$ where $x_1, x_2,\ldots, x_n$ are measured parameters whose uncertainties $\Delta x_1, \Delta x_2,\ldots, \Delta x_n$ are known, it is possible to calculate the accuracy associated to F in the following way:
$$\Delta F = \sum_{i=1}^{n}\left|\frac{\partial F(x_1, x_2, \ldots, x_n)}{\partial x_i}\right|\Delta x_i \tag{22}$$

Taylor expansion and covariance method (TECM): First, measured parameters $x_1, x_2,\ldots, x_n$ whose standard deviations $\sigma_1, \sigma_2,\ldots, \sigma_n$ are a known function of several variables $F(x_1, x_{2,\ldots,} x_n)$ computed from the parameters were considered.

Second, Gaussian noise with zero mean value for the parameters and the function F were introduced as follows:
$$F(x_1, x_2, \ldots, x_n) + e_F = F\left(x_1 + e_{x_1}, e_{x_2} + e_{x_2}, \ldots, x_n + e_{x_n}\right) \tag{23}$$

where e_F and e_{xi} are the random noise observed on the function F and the parameters x_i, respectively. Third, a linear relationship between the random noises e_F and e_{xi} using a first order Taylor's development was assumed:
$$F\left(x_1 + e_{x_1}, x_2 + e_{x_2}, \ldots, x_n + e_{x_n}\right) = F\left(x_1, x_2, \ldots, x_n\right) + \sum_{i=1}^{n} e_{x_i}\frac{\partial F\left(x_1, x_2, \ldots, x_n\right)}{\partial x_i} + o\left(\left\|x_1, x_2, \ldots, x_n\right\|\right) \tag{24}$$

Combining Equations (23) and (24) gives:
$$e_F \approx \sum_{i=1}^{n} e_{x_i}\frac{\partial F\left(x_1, x_2, \ldots, x_n\right)}{\partial x_i} \tag{25}$$

Equation (25) could be written as matrix expression:

$$e_F \approx G\left[e_{X_i}\right] \tag{26}$$

where $$G = \left[\frac{\partial F(x_1, x_2, ..., x_n)}{\partial x_1} \quad \frac{\partial F(x_1, x_2, ..., x_n)}{\partial x_2} \quad \dots \quad \frac{\partial F(x_1, x_2, ..., x_n)}{\partial x_n}\right] \tag{27}$$

Fourthly, according to [Beck and Arnold, 1982], the covariance of e_F is expressed:

$$\mathrm{cov}(e_F) = G\,\mathrm{cov}\left[e_{x_i}\right]G^T \tag{28}$$

Furthermore, if all the measured parameters are independent, the covariance matrix can be written in diagonal form whose values are equal to the square of the standard deviation, therefore the standard deviation of the function F can be determined:

$$\sigma_F = \sqrt{\mathrm{cov}(e_F)} = \sqrt{\sum_{i=1}^{n}\left(\frac{\partial F(x_1, x_2, ..., x_n)}{\partial x_i}\right)^2 \sigma_i^2} \tag{29}$$

Developments of the accuracy computations for porosity, two-phase and three-phase saturations are listed in [Caubit, 2004].

EXPERIMENTS

In this section, a gas-oil gravity drainage experiment followed by a tertiary waterflood performed on a long, intermediate-wet core is described. *In situ* saturation measurement and associated accuracy are presented in details at all stages of the experiment.

Experimental

- Porous medium:

The porous medium used in this study was Aerolith 10®, an artificial consolidated core, available in circular cross section, D=0.05m and L=1m. This porous medium is homogeneous and water-wet, has a 40% porosity and approximately $8.10^{-12}m^2$ permeability.

- Fluids:

The oil used was a mineral refined paraffin (Marcol 52 from Esso). The water phase was a brine containing 50g/l Sodium Iodide (NaI). The salt was added to the water phase in order to increase the gamma-ray attenuation coefficient and improve attenuation contrast with the oil phase. The gas used in this study was air and its attenuation coefficient was considered to be negligible compared to the oil and water phases. Physical properties of the fluids are given in Table 2.

- Experimental setups:

The two experimental setups shown in Figures 2 and 3 were used for the gravity drainage and the tertiary waterflood.

Experimental procedure

A gas-oil gravity drainage experiment was followed by a tertiary waterflood performed on a long core. Wettability was altered by an ageing process. The results were distinguished between static and dynamic measurements. For static measurements (porosity and stabilized saturation profiles) counting times were equal to 600s for the Americium source and 360s for Caesium source. For dynamic measurements (saturation profiles during the flow processes), counting time for Americium source was 120s and 30s for Caesium source.

The experimental procedure was as follows:
1. Core preparation: The core was epoxy coated and inlet and outlet devices were mounted with valves.
2. Dry counting: The first gamma-rays counting (N_1) was performed with the two sources of energy along the entire vertical axis of the core.
3. Porosity measurement: Gamma-rays were counted (N_2) along the fully brine saturated core in order to determine the local porosity profile.
4. Permeability measurement: Brine was injected into the core at different flow rates while measuring the pressure drop. Permeability k_w was determined using Darcy's law.
5. Primary drainage: Oil was injected from the bottom at a constant flow rate ($300cc.h^{-1}$) to displace brine down to irreducible water saturation (S_{wi}). Oil production and pressure drop were measured continuously. Gamma-rays were counted (N_3) and the saturation profile was determined.
6. Ageing process: Mineral oil was replaced by crude oil in a miscible process. The core was then maintained at 80°C in an oven for 69 days. Crude oil was then displaced by mineral oil in a miscible displacement. At this stage, the core initially water-wet, was weakly oil-wet [Pedrera, 2002].
7. Gravity drainage: Higher and lower valves were opened and oil was drained by gravity effect. Saturation profiles (dynamic) and oil recovery were measured during the entire experiment. At the end of the drainage process, when oil production stopped, saturation profiles were measured under static conditions (N_4).
8. Tertiary waterflood: Water was injected at a constant flow rate ($9cc.h^{-1}$) to displace oil and gas. Saturation profiles, fluid recoveries and pressure drop were measured continuously. Static saturation profiles were measured at the end of experiment (N_4).

Experimental data and accuracy

The accuracy of porosity and static saturation measurements of residual saturation after gravity drainage and tertiary waterflood was verified.

Porosity: Americium vs.Caesium

The porosity profiles measured by Americium and Caesium sources are plotted in Figure 4a. The mean values are 0.40 for Am and 0.42 for Cs. Moreover, the porosity profiles measured with Cs are more scattered than the Am porosity profiles. In Figure 4b, the accuracy of measurements is presented. It clearly appears that Americium measurements are more accurate than the Caesium measurements. This is mainly due to the contrast between the water attenuation coefficient of Am and Cs which is higher for Americium energy than for Caesium energy (see Table 2). It is important to note the difference between the mean Am and Cs porosity values because they were both used for three-phase measurement in Equations (19) and (21) which increased the three-phase saturation accuracy

Saturation data and accuracy: static and dynamic measurement

Primary drainage (water/oil)

Comparison between the two-phase Americium measurement method and three-phase measurement method:
In Figure 5a, the saturation profiles measured with Americium device (for two phase flow) and the dual energy system (for three-phase flow) are compared. The first method, give the best results as long as gas saturation is equal to zero. These results are confirmed by the data plotted in Figures 5b and 5c. Moreover, the two saturation measurement methods give similar results. Indeed, the water saturation profiles are almost identical using the two

methods. Nevertheless the main difference concerned the oil saturation profile which is more scattered with the three-phase measurement method.
Taylor expansion and covariance method (TECM):
Figure 5b shows that oil saturation is the least accurate. However, the differential method (DM), shown in Figure 5c, demonstrates that gas saturation is the least accurate. These results follow logically because the differential method cumulates all the errors of gas saturation ($\Delta S_g^{3\varphi} = \Delta S_o^{3\varphi} + \Delta S_w^{3\varphi}$), yet these results do not take into consideration the phenomena observed in the saturation profiles plotted in Figure 5a.

Gravity drainage

The dynamic saturation profiles measured during the gravity drainage process and comparison of the results with the global mass balance are presented. Finally, the final profile and its measurement accuracy are presented.
Dynamic oil saturation profiles:
The core can be divided in two zones during a gravity drainage process: the upper zone, where there is a three-phase flow configuration (air/oil in presence of connate water) and the lower zone where only oil and water are present. Optimization of measurement accuracy was based on a “front tracking” technique. The dual energy system was used in the upper zone of the core while the Americium source alone was used in the lower zone. In Figure 6a, dynamic profiles measured using only the dual energy system are presented. Oil saturation profiles are very scattered. In Figure 6b, oil saturation profiles with the present method of measurement accuracy optimization are presented. Scatter is strongly reduced. Moreover, in order to confirm the reliability of the three-phase saturation profile accuracy, the oil recovery deduced from the saturation profiles was compared to the experimental oil recovery. The two curves agreed well.
Static three-phase saturation profiles:
As for primary drainage, Figure 7b indicates that TECM is more representative than DM of the experimental phenomena observed in Figure 7a. Indeed, for three-phase measurement, only TECM shows that the oil saturation profile is the most scattered because DM cumulated all the error of gas saturation. Moreover, in Figure 9b saturation accuracy increases when the amount of gas increases.

Tertiary waterflood

Dynamic saturation profiles:
There was very good agreement between water/oil volume recoveries deduced from the volume read on graduated tubes and recoveries deduced from saturation profiles which confirmed the reliability of the dynamic saturation profiles measured by the dual energy system.
Static three-phase saturation profiles:
In tertiary waterflood (Figures 8a and 8b) the same features described previously (for primary drainage and gravity drainage) in term of accuracy calculation (TECM and DM) were found.

CONCLUSIONS

In this study, an improvement in the dual-energy system used to measure three-phase saturations is presented. The focus was placed on accuracy determination in order to optimize the measurement procedure. Different counting times were used to measure static (porosity, final saturation profiles) and dynamic (transient saturation profiles) properties. Moreover, a single source was used when two-phase flow occurred while a dual-energy system was used only for three-phase saturation.

Gravity drainage followed by a tertiary waterflood experiment is presented from which the following conclusions can be drawn.

Porosity measurement is more accurate with Americium than Caesium.

Determination of irreducible water saturation profile at the end of the primary drainage is more accurate with the Americium two-phase device than with the Americium-Caesium three-phase device.

A “front tracking” procedure improves accuracy measurement during the gravity drainage process and the tertiary waterflood.

All these observations were confirmed by the computation of accuracy using the Taylor expansion and a covariance method which provided results in good agreement with the experimental phenomena observed.

The dual-energy system for measuring three-phase saturation remains an interesting technique considering its price, availability and accuracy assuming that the experimental procedure is optimized.

Acknowledgments

We thank Total for permission to publish this paper.

References

1. Angulo-Jaramillo R., Caractérisation hydrodynamique de sols déformables partiellement saturés : Etude expérimentale à l’aide de la spectrométrie gamma doubles sources, Ph.D : Mécanique INPG, 1989.
2. Barataud F., Moyne C. and Stemmelen D., Measurement of soil water diffusity of an undisturbed forest soil using dual energy gamma radiation technique, Soil Science, 1999 ; Vol.164 No.7, p.493-502.
3. Barroux C., Bouvier L., Maquignon P. Thiebot B., Alternate dual-energy gamma-ray attenuation technique: a new tool for three-fluid satuartion measurements in IOR flood experiments, 6th European Symposium On IOR, Stavanger, 1991.
4. Beck, J. V. and. Arnold K. J, Parameter estimation in engineering and science, Ed. Wiley, 1977.
5. Caubit, C., Influence de la mouillabilité sur les saturations limites lors d’écoulement triphasique en milieu poreux, Ph.D : Thesis, U. of Bordeaux, 2004.
6. Ferrand L. A., Milly P. C. D. and Pinder G. F., Dual-Gamma Attenuation for the Determination of Porous Medium Saturation With Respect to Three Fluids, Water Resources Research, Vol.22, No.12, p. 1675-1663, 1986.
7. Naylor P. and Frorup M., Gravity-Stable Nitrogen Displacement of Oil, SPE 19641, 1989
8. Nofziger D. L. and Swartzendruber D., Material and contents of binary physical mixture as measured with dual energy beam of gamma-rays, Journal of Applied Physics, Vol.45, No. 12, 1974.

9. Oak M. J. and Ehrlich R., A New X-Ray Absorption Method for Measurement of Three-Phase Relative Permeabilitiy, SPERE, 1988, p199-206.
10. Pedrera B., Influence de la mouillabilité sur les propriétés polyphasiques d'un milieu poreux lors d'un drainage par gravité, Ph.D : Thesis, U. of Bordeaux, 2002
11. Roussel J. C. and Chardaire-Rivière C., Use of a high magnetic field to visualize fluids in porous media By MRI, SCA 9112, 1991.
12. Sahni A., Measurement of three-phase relative permeability during gravity drainage using CT Scan, Ph.D : Thesis, Stanford U., 1998
13. Stroosnijder J. and De Swart J. G., Column scanning with simultaneous use of ^{241}Am and ^{137}Cs gamma radiation, Soil Science, 1974; Vol.118 No.2, p.61-68.
14. Tait W. H. Radiation Detection, Ed. Butterworth, 1980.
15. Vizika O. and Kalaydjian F., A new method to measure water, oil and gas saturation in three-phase gas injection, SCA 9505, 1995.

Nomenclature

A	Activity (Bq)
A_o	Initial Activity (Bq)
I	Intensity (eV)
k_r	Relative permeability
l	Length of the porous media (m)
N_i^j	j Counting in i condition
N_0^j	j Counting of the emitted radiation
P_c	Capillary pressure (Pa)
S_i^j	i Saturation for j measurement
S_b	Gamma beam cross section (m^2)
$T_{1/2}$	Half life (Radioactive source)
V_i	Volume of the phase i (m^3)
V_p	Pore volume (m^3)
V_T	Total volume (Porous media) (m^3)
α_i	Mass attenuation coefficient (m^2g^{-1})
ΔX	Error on the parameter X
ϕ	Porosity
ν	Radiation frequency (s^{-1})
ρ_i	Density of the phase i (gm^{-3})
σ_i^j	i Standard deviation for j measurement
ξ_i^j	i linear attenuation coefficient for j (m^{-1}) source

Subscript:

g	gas
o	oil
w	water
1	Dry
2	Brine saturated
3	Two-phase flow
4	Three-phase flow
s	solid

Upscript:

Am	Americium
Cs	Caesium
2φ	Two-phase measurement
3φ	Three-phase measurement

Tables and Figures

Radionuclide	Energy	Activity	Half Life
Americium	59.6 keV	300 mCi	458 years
Caesium	660 keV	20 mCi	30 years

Table 1: Americium and Caesium source properties

	Density ($kg.m^{-3}$)	Viscosity (Pa.s)
Brine 50 gl^{-1}	1042	$1.0\ 10^{-3}$
Mineral oil Marcol 52	831	$11.3\ 10^{-3}$
Air	1.29	$1.8\ 10^{-5}$
Crude oil	790	-

Table 2: Fluid properties

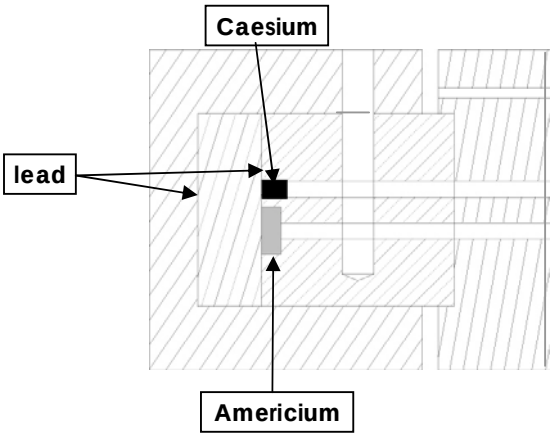

Figure 1: The source holder

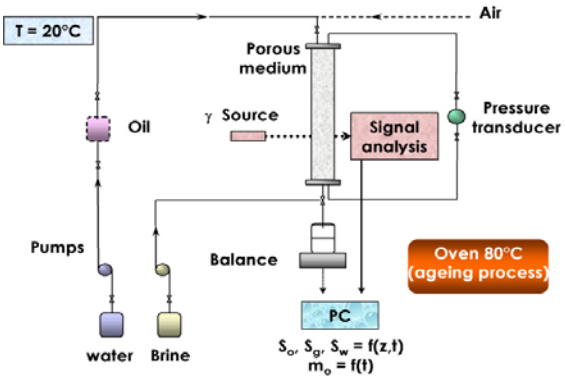

Figure 2: Gravity drainage measurement apparatus

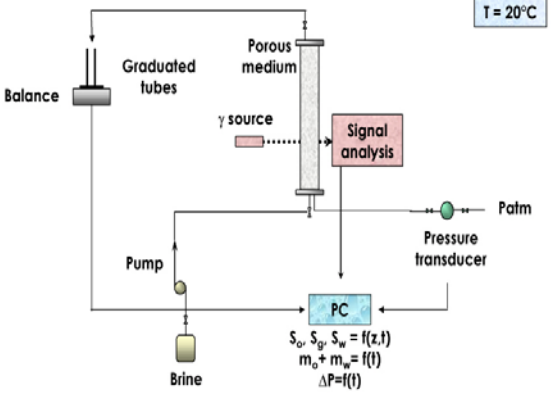

Figure 3: Tertiary waterflood measurement apparatus

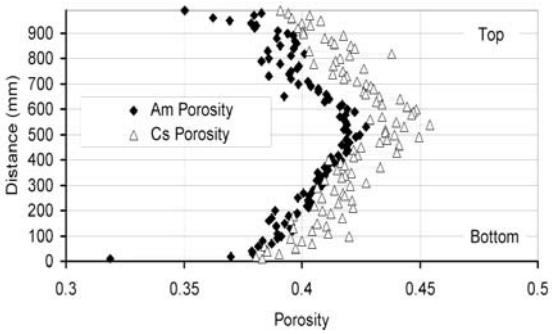

Figure 4a: Comparison between Americium and Caesium porosity

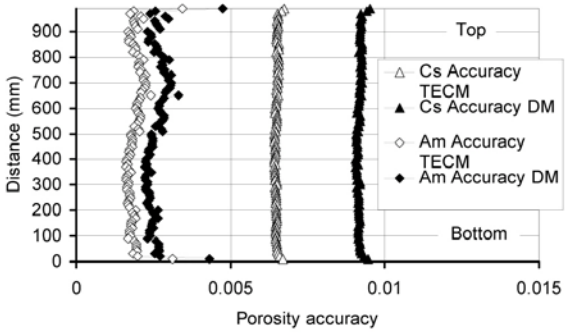

b)

*Figure 4b: Porosity accuracy: Taylor expansion and covariance method **TECM** and Differential method **DM***

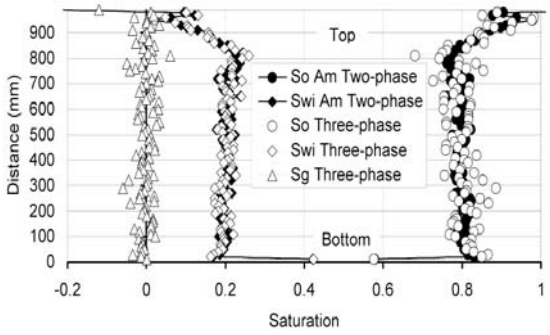

Figure 5a: Comparison between Americium two-phase measurement and three-phase measurement

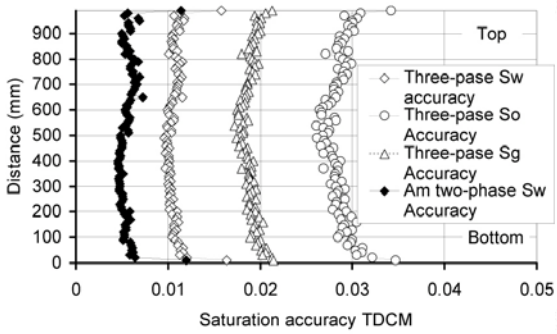

*Figure 5b: Saturation accuracy: **TECM***

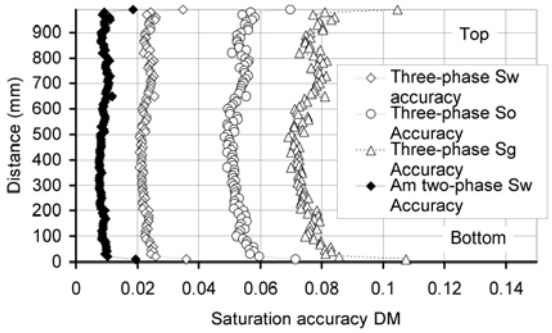

*Figure 5c: Saturation accuracy: **DM***

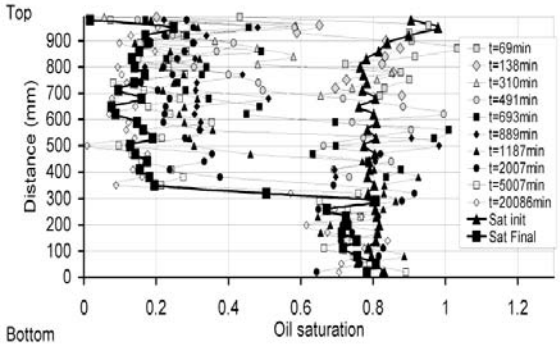

Figure 6a: Raw three-phase oil saturation profiles during gravity drainage

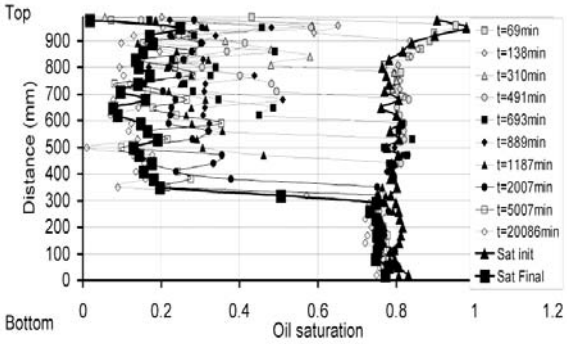

Figure 6b: Corrected three-phase oil saturation profiles during gravity drainage

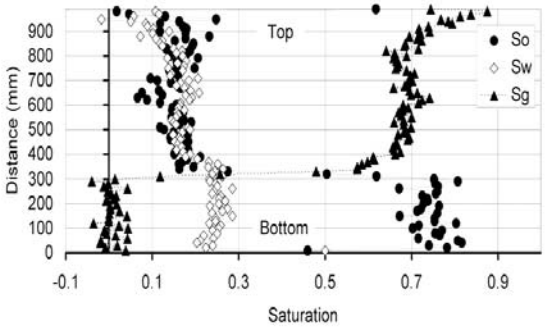

Figure 7a: Static three-phase saturation profiles at the end of the Gravity Drainage

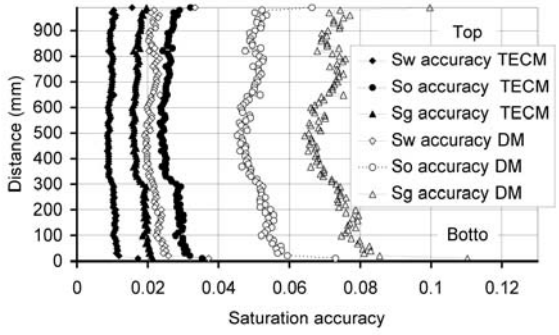

b)

*Figure 7b: Saturation accuracy: **TECM** and **DM***

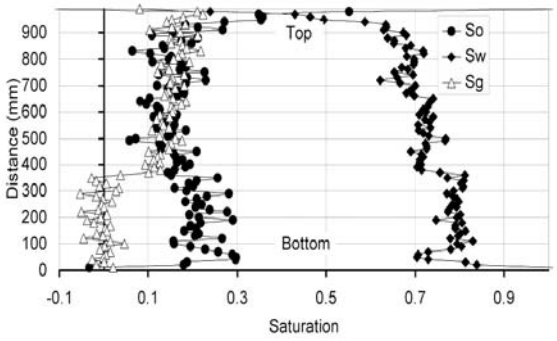

Figure 8a: Static three-phase profiles at the end of tertiary waterflood

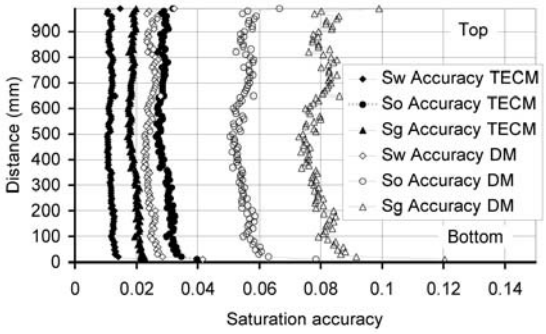

Figure 8b: Saturation accuracy:

TECM** and **DM